Quaternary Research 71 (2009) 453–464

Contents lists available at ScienceDirect

Quaternary Research

journal homepage: www.elsevier.com/locate/yqres

Modern and late Quaternary clay mineral distribution in the area of the SE Mediterranean Sea

Yvonne Hamann *[,1], Werner Ehrmann, Gerhard Schmiedl [2], Tanja Kuhnt [3]

Universität Leipzig, Institut für Geophysik und Geologie, Talstrasse 35, 04103 Leipzig, Germany

ARTICLE INFO

Article history:
Received 25 October 2007
Available online 28 February 2009

Keywords:
Levantine Sea
Clay minerals
Late Quaternary
Nile River
Palaeoclimate

ABSTRACT

The present-day clay mineral distribution in the southeastern Levantine Sea and its borderlands reveals a complex pattern of different sources and distribution paths. Smectite dominates the suspended load of the Nile River and of rivers in the Near East. Illite sources are dust-bearing winds from the Sahara and southwestern Europe. Kaolinite is prevalent in rivers of the Sinai, in Egyptian wadis, and in Saharan dust. A high-resolution sediment core from the southeastern Levantine Sea spanning the last 27 ka shows that all these sources contributed during the late Quaternary and that the Nile River played a very important role in the supply of clay. Nile influence was reduced during the glacial period but was higher during the African Humid Period. In contrast to the sharp beginning and end of the African Humid Period recorded in West African records (15 and 5.5 ka), our data show a more transitional pattern and slightly lower Nile River discharge rates not starting until 4 ka. The similarity of the smectite concentrations with fluctuations in sea-surface temperatures of the tropical western Indian Ocean indicates a close relationship between the Indian Ocean climate system and the discharge of the Nile River.

Introduction

As part of the Eastern Mediterranean Sea, the Levantine Sea is an intercontinental basin, semi-enclosed by land. The main sources of fluviatile sediments are permanent rivers draining southeastern Europe, Turkey and the eastern part of Africa. Large amounts of aeolian sediment are blown into the Levantine Sea, the Sahara being the major source. These transport processes are tightly coupled to the climate variability of the borderlands, particularly including changes in precipitation and erosion potential of the Nile River catchment, and wind strength and deflation potential of the Saharan desert. During the late glacial and Holocene periods, central and northern Africa experienced pronounced humidity changes linked to the African monsoon system. Lake levels and various proxy records documented the onset of humid conditions at around 15 ka (review in Gasse, 2000). This so-called African Humid Period (AHP) lasted until approximately 5.5 ka (deMenocal et al., 2000a). Enhanced Nile River runoff during this time has been associated with stratification of surface water masses and reduced deep-water formation in the Mediterranean Sea, leading to the formation of sapropel S1 (e.g., Rossignol-Strick et al., 1982). Various studies have focused on the understanding of these land–ocean linkages on orbital time-scales. However, little is known about the impact of abrupt climate changes on terrigenous input and sedimentation processes of the Levantine Sea.

A variety of sedimentological and geochemical methods have been applied to characterize source areas, transport processes and distribution of terrigenous sediment in the marine environment. Past variations in bottom current speed, wind strength, and the mode of transport can been reconstructed by end-member modelling of grain-size distributions (e.g., Stuut and Lamy, 2004). In the Mediterranean Sea, Moreno et al. (2002) and Hamann et al. (2008) applied this method to late glacial and Holocene sediments in order to distinguish between fluviatile and wind-derived material. In addition, Sr and Nd isotope analyses of terrigenous material have been used to obtain information on sediment sources and to constrain transport paths of detrital material (e.g., Tütken et al., 2002). Sr and Nd isotopic ratios also provide useful information of changes in oceanic circulation patterns and pathways in sediment transport. With this toolbox, Weldeab et al. (2002a,b) were able to characterize the surface sediments in the Eastern Mediterranean Sea and to distinguish provenances and pathways of suspended matter. The type and the proportions of individual clay minerals in sediments are linked to the terrigenous sediment supply, the source rocks, weathering conditions on land and transport mechanisms (e.g., Biscaye, 1965).

Clay mineral studies in the Mediterranean Sea focus mainly on the clay mineral distribution in marine and terrestrial surface sediments of the eastern basins and their hinterland (e.g., Venkatarathnam and

* Corresponding author. Fax: +41 44 6321080.
E-mail address: yvonne.hamann@erdw.ethz.ch (Y. Hamann).
[1] Present address: ETH Zürich, Geologisches Institut, Sonnegstrasse 5, 8092 Zürich, Switzerland.
[2] Present address: Universität Hamburg, Institut für Geologie und Paläontologie, Bundesstrasse 55, 20146 Hamburg, Germany.
[3] Present address: Université d'Angers, Laboratoire d'Etude des Bio-indicateurs Actuels et Fossiles, 2 Boulevard Lavoisier, 49045 Angers Cedex, France.

0033-5894/$ – see front matter © 2009 University of Washington. All rights reserved.
doi:10.1016/j.yqres.2009.01.001

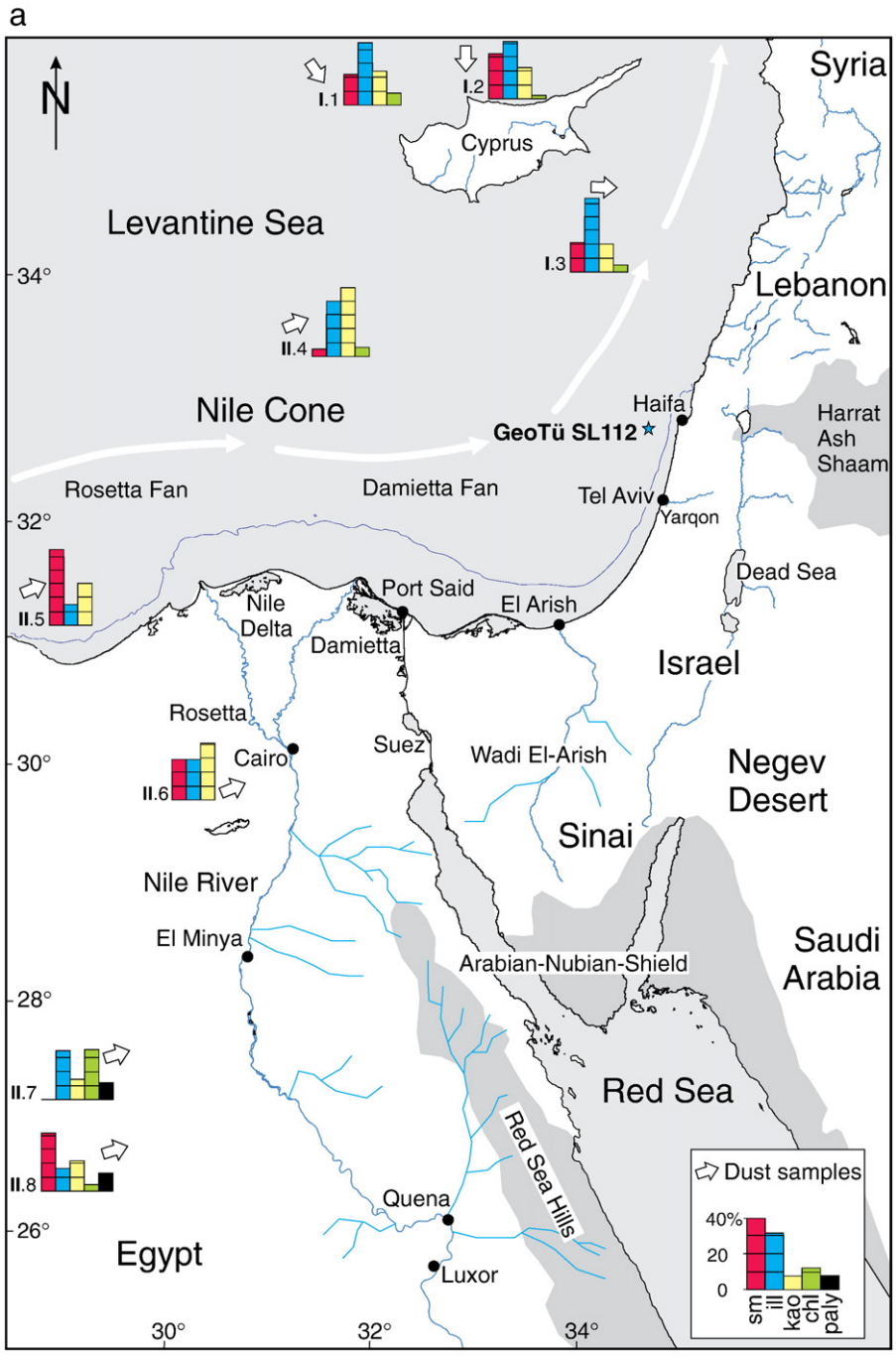

Figure 1. (a) Map of the southeastern Levantine Sea and adjacent areas with location of sediment core GeoTü SL112. The distribution of the main clay mineral groups smectite (sm), illite (ill), kaolinite (kao), chlorite (chl) and palygorskite (paly) in recent dust samples (arrows) is shown (various sources, Table 1). For exact location of samples II.7 and II.8 see Table 1. Present-day sea-surface circulation is represented by white elongated arrows (Pinardi and Masetti, 2000), 100-m depth contours are given. (b) Distribution of the main clay mineral smectite (sm), groups illite (ill), kaolinite (kao) and chlorite (chl) in marine surface samples (asterisks) and recent river/wadi samples (arrows). The data have been compiled from various sources (see Table 1).

Ryan, 1971; Chester et al., 1977; Maldonado and Stanley, 1981; Aksu et al., 1995; Sandler and Herut, 2000; Ehrmann et al., 2007a,b). These studies highlight the Nile River as the dominant sediment source, which provides large quantities of sediment to the southeastern part of the basin. In contrast, aeolian input from the Sahara and the riverine supply of smaller rivers and wadis are of minor importance when compared to the suspended material derived by the Nile. The Nile River originates in central-east Africa and incorporates up to 90% of its clay-rich suspension load close to its source (Adamson et al., 1980). During the flow from the catchment area to the delta, the river passes through different climate zones, ranging from a cool and humid climate in the Ethiopian highlands to the desert climate in Egypt. Thus, the Nile River is highly sensitive to changes in precipitation patterns in central Africa. Hence, the clay mineral assemblage of the Nile load appears to be a useful indicator for environmental changes and weathering processes in the source area.

In the present study, we compile published clay mineral data from the southeastern Levantine Sea and its borderlands. We give an overview on recent clay mineral supply, source areas, transport and sedimentation processes, and distribution patterns in marine surface sediments. This knowledge is then applied to the palaeoclimatic interpretation of a high-resolution clay mineral data set from the

https://doi.org/10.1016/j.yqres.2009.01.001 Published online by Cambridge University Press

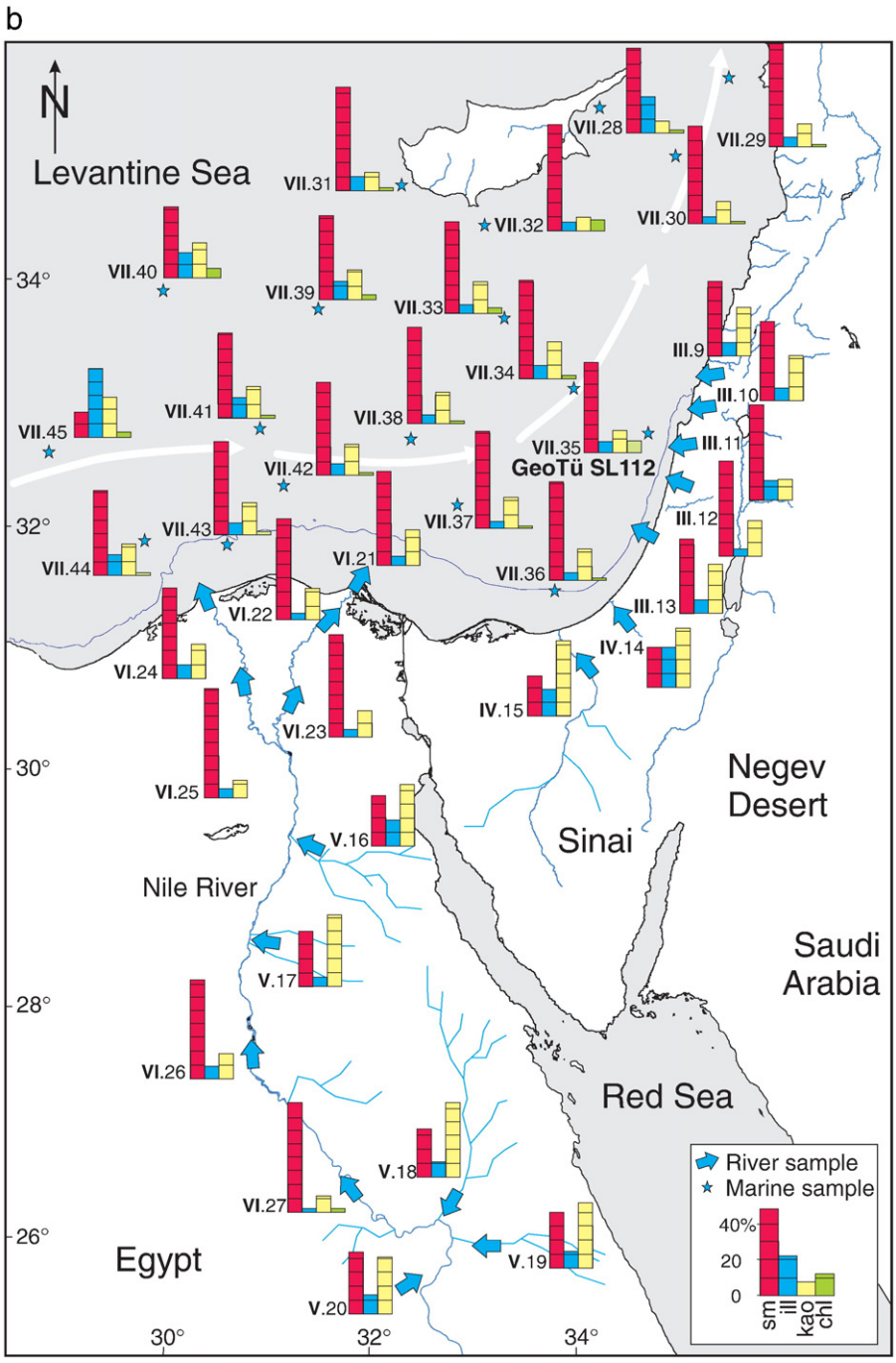

Figure 1 (*continued*).

Israel continental margin. The investigated sediment core is located downstream the Nile River outflow, ideally positioned to record the orbital and suborbital climate variability in the Nile catchment area over the last ca. 27 ka.

Environmental setting

Climatic conditions and oceanography

The Eastern Mediterranean Sea and the surrounding mainland are controlled by different climate regimes. A temperate and humid to semi-arid climate is characteristic for wide parts of southeast Europe and Turkey, which is influenced by the North Atlantic Oscillation (NAO; e.g., Hurrell et al., 2003). The Near East is located in the climatic transition zone between the temperate and humid conditions in the north and arid conditions with deserts in the south. The northern part of Africa is dominated by semiarid to arid tropics and subtropics, while the central areas are characterized by semi-humid conditions and cold tropics (e.g., Highland of Ethiopia). The precipitation and drought patterns of the northern African continent are related to a complex interplay between global climate patterns and regional phenomena. Large-scale moisture availability is related to the annual migration of the Intertropical Convergence Zone (ITCZ) and is influenced by the African monsoon system, which is connected to the pan-tropical El Niño–Southern Oscillation (ENSO; e.g., Janicot et al., 1997; Schott and McCreary, 2001). The Indian Ocean and the adjacent regions are affected by interannual Indian Ocean Dipole (IOD) events (e.g., Saji et al., 1999; Webster et al., 1999; Abram et al., 2007). This coupled

https://doi.org/10.1016/j.yqres.2009.01.001 Published online by Cambridge University Press

ocean–atmosphere phenomenon displays periodic oscillations related to changes in the sea-surface temperature (SST) that control the availability of moisture. The relationship between the IOD, the monsoon system and ENSO is still a matter of intense debate (Saji and Yamagata, 2003).

Evaporation rates exceed the freshwater influx by precipitation and river supply in the arid Eastern Mediterranean Sea. The salinity of the surface water masses in the Levantine Sea is 38‰ to >39‰ (Wüst, 1960). The mean water temperature ranges between 16°C during winter and up to 27°C during summer (Wüst, 1960, 1961).

The general circulation pattern exhibits a counterclockwise current of the Eastern Mediterranean Surface Water (MSW) (e.g., Pickard and Emery, 1982; Pinardi and Masetti, 2000; Fig. 1a). During winter, in times of intensive evaporation, Levantine Intermediate Water (LIW)

Table 1
Compilation of published clay mineral data from river channel and wadi surface sediments, dust samples and marine surface sediments in the southeastern Levantine Sea and the adjacent mainland

No. Investigation area	*n*	Smectite (%)	Illite (%)	Kaolinite (%)	Chlorite (%)	Palygorskite (%)	References
I. Northern Dust Assemblage							
1 NW of Cyprus (group B)	6	22	45	24	<10	n.d.	Chester et al. (1977)
2 N of Cyprus (group A)	4	33	41	23	<5	n.d.	Chester et al. (1977)
3 SE of Cyprus (group C)	4	21	54	20	<7	n.d.	Chester et al. (1977)
II. Saharan Dust Assemblage							
4 SE Levantine Sea (group D)	10	<5	40	50	<8	n.d.	Chester et al. (1977)
5 N Egypt, Libya	19	55	15	30	n.d.	*[1]	Ganor and Mamane (1982) *after* Ganor (1975)
6 Cairo	2	29	29	42	n.d.	n.d.	Stanley and Wingerath (1996)
7 Saharan dust sample (N Algeria)	n.d.	n.d.	36	15	36	10–15	Paquet et al. (1984)
8 Saharan dust sample (S of Hoggar)	n.d.	43	10–25	20–25	5	10–15	Paquet et al. (1984)
III. Near East Assemblage							
9 N Israeli coast (clay assemblage III)	11	40–69	Variable	>30	*[2]	n.d.	Stanley et al. (1997)
10 N of Haifa	5	58	9	33	n.d.	n.d.	Stanley and Galili (1996)
11 S of Haifa (clay assemblage II)	9	>70	<10–19	<20	*[2]	n.d.	Stanley et al. (1997)
12 N of Tel Aviv (clay assemblage I)	5	>70	<10	20–29	*[2]	n.d.	Stanley et al. (1997)
13 S of Tel Aviv (clay assemblage III)	10	40–69	Variable	>30	*[2]	n.d.	Stanley et al. (1997)
IV. Sinai Assemblage							
14 E of El Arish (JM 920–922)	3	29	29	42	*[2]	n.d.	Stanley et al. (1997)
15 El Arish (YN-3031)	1	28	19	53	*[2]	n.d.	Stanley et al. (1997)
V. Egyptian Wadi Assemblage							
16 S of Cairo (Wadi-10)	1	37	18	45	n.d.	n.d.	Stanley and Wingerath (1996)
17 N of El Minya (Wadi-12, 13)	2	40	7	53	n.d.	n.d.	Stanley and Wingerath (1996)
18 NE of Qena (Wadi-49)	1	34	11	55	n.d.	n.d.	Stanley and Wingerath (1996)
19 S of Qena (Wadi-58 to 60)	3	40	12	48	n.d.	n.d.	Stanley and Wingerath (1996)
20 W of Luxor	1	45	14	41	n.d.	n.d.	Stanley and Wingerath (1996) *after* Elgabaly and Khadr (1962)
VI. Nile Assemblage							
21 Damietta branch (Dam-1-CH-1990)	1	69	6	25	n.d.	n.d.	Stanley and Wingerath (1996)
22 Damietta branch	2	74	4	22	*[2]	n.d.	Stanley et al. (1997)
23 Damietta branch (Dam-3-CH, 1-CH)	2	76	5	19	n.d.	n.d.	Stanley and Wingerath (1996)
24 Rosetta branch (Ros-1-CH)	1	66	10	24	n.d.	n.d.	Stanley and Wingerath (1996)
25 Rosetta branch (Ros-3-CH, 4-CH)	2	81	6	13	n.d.	n.d.	Stanley and Wingerath (1996)
26 Nile, 30° to 27° latitude (CH 1, 3, 6, 9)	4	73	9	18	n.d.	n.d.	Stanley and Wingerath (1996)
27 N of Quena (Nile 1)	1	75–85*[3]	<5	10–15	<5	0	Sandler and Herut (2000)
VII. SE Levantine Sea Assemblage							
28 NE of Cyprus (sample 296)	1	62	26	9	<5	n.d.	Chester et al. (1977)
29 E of Cyprus	1	>70	<10	15–20	<3	n.d.	Venkatarathnam and Ryan (1971)
30 SE of Cyprus	1	60–70	<10	15–20	<3	n.d.	Venkatarathnam and Ryan (1971)
31 W of Cyprus (sample 236)	1	74	10	14	<5	n.d.	Chester et al. (1977)
32 S of Cyprus (samples 217, 219)	2	76	6	10	8	n.d.	Chester et al. (1977)
33 S of Cyprus	1	60–70	<10	20–25	3–5	n.d.	Venkatarathnam and Ryan (1971)
34 W of Haifa (sample 30)	1	>70	<10	20–25	<3	n.d.	Maldonado and Stanley (1981)
35 W of Haifa (GeoTü SL112)	1	66	8	16	9	n.d.	This study
36 N of El Arish (sample 48)	1	>70	<10	20–25	<3	n.d.	Maldonado and Stanley (1981)
37 Damietta Fan (sample 47)	1	>70	<10	20–25	<3	n.d.	Maldonado and Stanley (1981)
38 Damietta Fan	1	60–70	<10	20–25	<3	n.d.	Venkatarathnam and Ryan (1971)
39 Central Levantine Sea (sample 33)	1	60–70	10–20	20–25	3–5	n.d.	Maldonado and Stanley (1981)
40 Central Levantine Sea	1	40–60	10–20	20–25	5–7	n.d.	Venkatarathnam and Ryan (1971)
41 Central Nile Cone	1	60–70	10–20	20–25	<3	n.d.	Venkatarathnam and Ryan (1971)
42 Central Nile Cone (samples 7, 8)	2	60–70	<10	20–25	<3	n.d.	Maldonado and Stanley (1981)
43 Rosetta Fan (sample 39)	1	60–70	<10	20–25	<3	n.d.	Maldonado and Stanley (1981)
44 Rosetta Fan	1	40–60	10–20	25–30	3–5	n.d.	Venkatarathnam and Ryan (1971)
45 Rosetta Fan	1	60–70	10–20	20–25	<3	n.d.	Venkatarathnam and Ryan (1971)

Values indicate mean concentrations and concentration ranges, respectively, of the individual clay minerals *n* number of samples; n.d. not determined; *[1] concentrations not shown separately, low amounts within illite and *[2] kaolinite, respectively; *[3] termed as illite-smectite phase.
The locations of samples are shown in Figures 1 and 2.

https://doi.org/10.1016/j.yqres.2009.01.001 Published online by Cambridge University Press

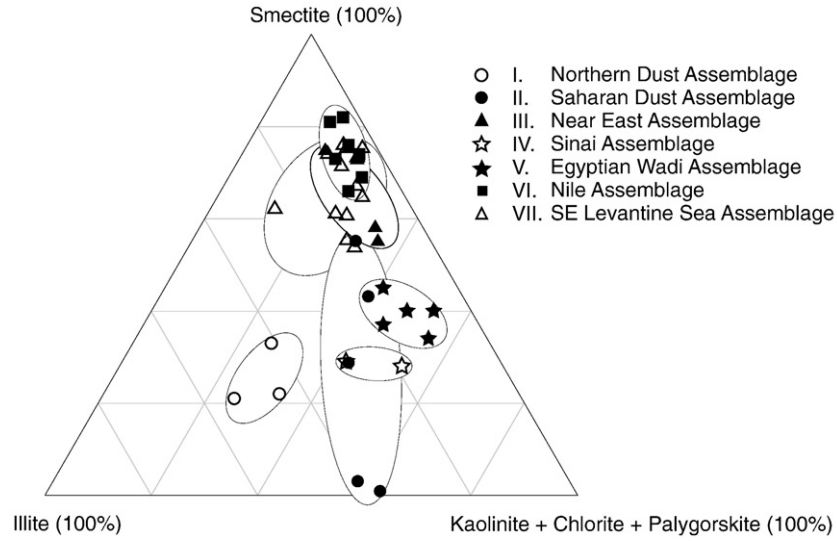

Figure 2. Ternary diagram of the major clay mineral groups smectite, illite and kaolinite + chlorite + palygorskite. Distributions are grouped in clusters reflecting the individual clay mineral assemblages.

forms, sinks to a depth between 200 m and up to 600 m in the northwestern part of the Levantine Sea, and flows towards the west into the western Mediterranean Sea (Wüst, 1961; Pickard and Emery, 1982; Malanotte-Rizzoli and Hecht, 1988). Eastern Mediterranean Deep Water (EMDW) forms during winter in the southern Adriatic Sea and the southern Aegean Sea and fills the Ionian and Levantine basins below 800 m (Wüst, 1961; Klein et al., 1999).

Sediment supply into the southeastern Levantine Sea

The Nile River is the dominant sediment source for the southeastern Levantine Sea (Fig. 1a; Venkatarathnam and Ryan, 1971; Foucault and Meliérès, 2000). The majority of the silt- and sand-sized sediment is deposited in the Nile Delta, on the Nile Cone and along the shelf, whereas clay-sized sediments are dispersed in suspension by the MSW. The annual suspension load of the Nile River was estimated to $120–230 \times 10^6$ t/yr prior to the High Dam construction at Aswan in 1964 (Holeman, 1968; Milliman and Syvitski, 1992; Stanley and Wingerath, 1996; Garzanti et al., 2006). The Blue Nile and the Atbara are at present the most important sediment suppliers whereas the suspension load of the White Nile is comparatively small (Adamson et al., 1980; Williams et al., 2006). The sediment supplies from local wadis, that drain into the Nile River are of minor importance (Stanley et al., 1997). Wadi El-Arish drains the Sinai and provides sediments to the southeastern Levantine Sea, mainly during winter floods (Sandler and Herut, 2000). The Israeli Yarqon River is important for sediment supply because of its perennial character (Stanley et al., 1997; Sandler and Herut, 2000). Additional sediment comes from a number of ephemeral rivers, that drain the Near East. However, their sediment supply is only minor when compared to the supply by the Nile River.

Aeolian dust is a further sediment source for the Mediterranean Sea (e.g., Venkatarathnam and Ryan, 1971; Pye, 1992; Goudie and Middleton, 2001). Saharan dust is transported across the Mediterranean Sea to Europe and to the Middle East, and decreases in concentration with increasing distance from the source. Scirocco winds are the most important dust-bearing winds affecting the northern part of Africa. The Khamsin and the Simoom influence Egypt, the Near East and surrounding areas (Camuffo, 1993; Goudie and Middleton, 2001). These winds blow from the south and southwest (Joseph et al., 1973; Ganor and Mamane, 1982; Stanley and Wingerath, 1996) and transport large amounts of dust mainly during short events. Modern studies estimate a Saharan dust influx of up to 100×10^6 t/yr into the Eastern Mediterranean Sea (Goudie and Middleton, 2001). In particular, the northeasternmost sector of Egypt provides ca. 20×10^6 t/yr dust to the adjacent Levantine Sea (Ganor and Mamane, 1982). Aeolian influx comes also from the Near East by the Sharqiya winds (Saaroni et al., 1998). Winds from the northern and eastern Mediterranean hinterland are of minor importance and contain little (<10%) clay (Coudé-Gaussen, 1981).

Materials, methods and age model

In order to map the modern distribution pattern of clay minerals in the Levantine Sea and its surroundings, we compiled and generalized published data of various sources (Table 1). The data come from marine surface sediments retrieved by short gravity and box corers, from samples taken in rivers and wadi channels, and from dust samples. Bed load samples of the Nile River and the Nile Delta were collected after the construction of the Aswan High Dam. All studies were based on X-ray diffraction analyses of the clay fraction, and almost all used the method of Biscaye (1965) to calculate percentages of the individual clay minerals. We present the data in a generalized way (Figs. 1a, b, 2; Table 1), focusing on the major distribution patterns. In most cases we show mean concentrations of the clay minerals illite, smectite, kaolinite and chlorite, which we calculated from the original data sets (Table 1).

The analyzed gravity core GeoTü SL112 was recovered during RV Meteor cruise M51/3 in 2001 from the continental slope off Israel in the southeastern Levantine Sea at 32°44.52′N, 34°39.02′E in a water depth of 892 m (Hemleben, 2002; Fig. 1a). The core has a total length of 5.31 m and was sampled in intervals of 4 cm. The majority of the core consists of soft, water-rich, reddish grey to reddish brown mud and partly foraminifer-bearing mud with small amounts of sand. The $CaCO_3$ content fluctuates between 5% and 60%. The sediment is

Table 2
Data used for constructing the age model for the investigated core GeoTü SL112

Core depth cm	Uncalibrated ^{14}C yr BP (laboratory number)	Calendar age cal yr BP	Datum
0	0	0	Sediment surface
100	3035 ± 30 (KIA 28348)	2765–2743	^{14}C AMS dating
201	5505 ± 30 (KIA 28349)	5880–5860	^{14}C AMS dating
260	8365 ± 70 (KIA 30176)	8970–8690	^{14}C AMS dating
365	12,985 ± 60 (KIA 28350)	14,920–14,690	^{14}C AMS dating
498	20,930 + 130/− 120 (KIA 28351)	24,660–24,290	^{14}C AMS dating

https://doi.org/10.1016/j.yqres.2009.01.001 Published online by Cambridge University Press

moderately bioturbated. Faunal constituents are mainly foraminifera, pteropods, and fewer echinoderm fragments, sponge spicules, fragments of bivalves, radiolarians, ostracods, and fish remains. At a depth of 220–275 cm, the core contains sapropel S1, which was formed between approximately 9.6 and 6.5 ka (Kuhnt et al., 2008). It consists of dark reddish brown mud with moderate laminations and only minor bioturbation. The core exhibits a 2-mm-thick tephra layer within the sapropel at a depth of 260 cm.

The sample preparation and analyses for determining the clay mineralogy in core SL112 followed Ehrmann et al. (2007b). We used

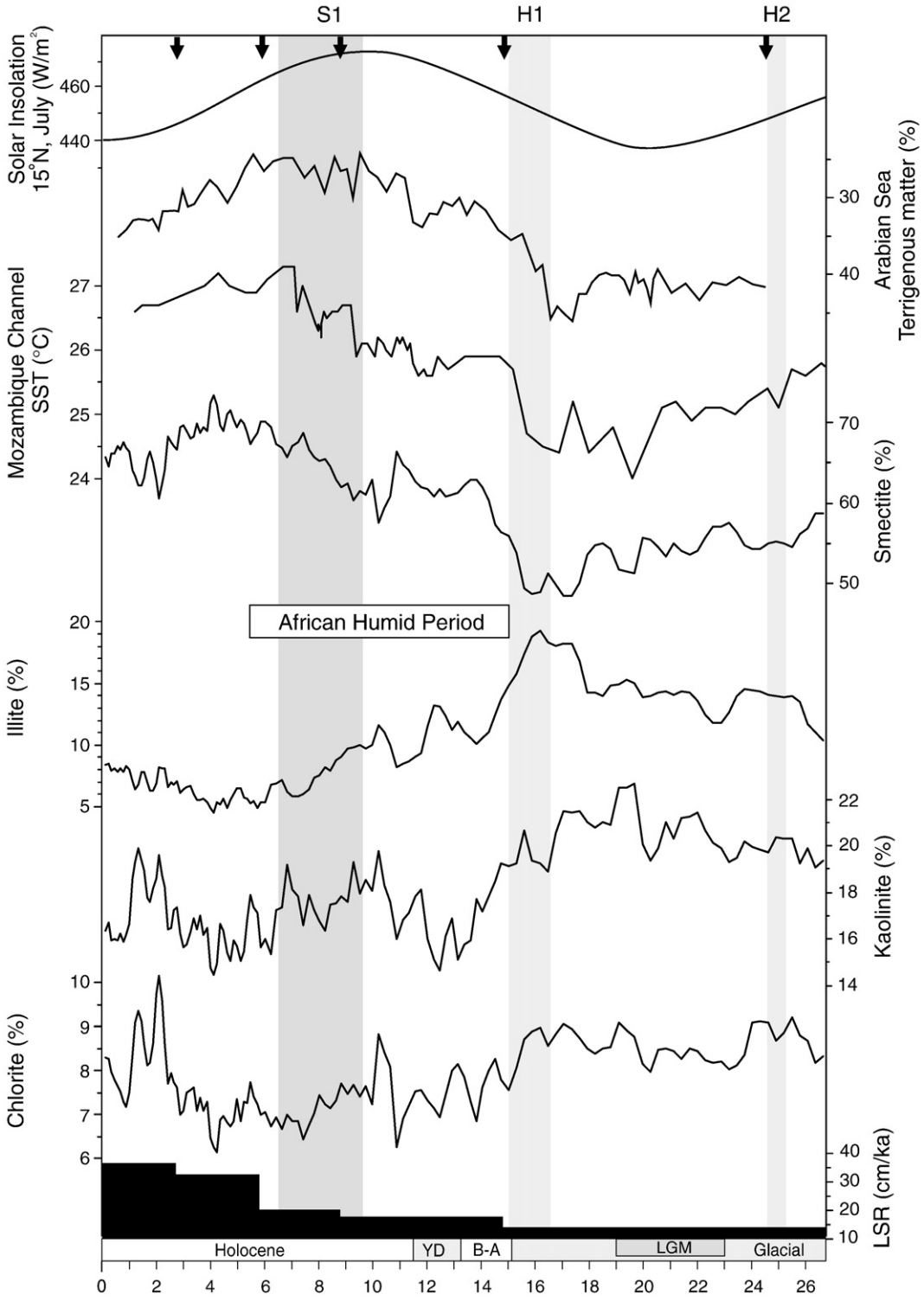

Figure 3. Late Quaternary variations in the concentrations of smectite, illite, kaolinite, chlorite (3-point-running means) and the linear sedimentation rate (LSR, in cm/ka) in core GeoTü SL112. Dark grey bar marks sapropel layer S1; light grey bars show Heinrich Events H1 and H2. The solar insolation in July at 15°N (W/m^2), the abundance of terrigenous matter in core 74KL from the western Arabian Sea (Sirocko et al., 1996; 14°19.26′N, 57°20.82′E) and the sea-surface temperature record of core MD79257 from the Mozambique Channel, western Indian Ocean (Bard et al., 1997; 20°24′S, 36°29′E) are shown for comparison. African Humid Period marked after deMenocal et al. (2000a). Arrows at the top indicate ^{14}C dates used for constructing the age model (Table 2), YD: Younger Dryas, B–A: Bølling–Allerød, LGM: last glacial maximum.

https://doi.org/10.1016/j.yqres.2009.01.001 Published online by Cambridge University Press

the weighting factors of Biscaye (1965) to calculate percentages of the clay minerals illite, smectite, kaolinite and chlorite. Palygorskite was detected in SL112 but could not be quantified because of its low concentrations.

The age model for core SL112 has been constructed based on five ^{14}C accelerator mass spectrometry (AMS) dates, analyzed at the Leibniz Laboratory for Age Determination and Isotope Research at the University of Kiel (Table 2). The analyses were carried out on well-preserved shells of mixed planktonic foraminifera (*G. ruber* white, *G. ruber* pink, *G. sacculifer*, *G. bulloides*, *G. siphonifera*, *O. universa*, *N. incompta*, *T. quinqueloba*). Reservoir ages were corrected after Siani et al. (2001), and ages were converted to calendar years with the radiocarbon calibration software of Fairbanks et al. (2005). According to the age model, the core has a basal age of 26.95 cal ka BP.

The raw sedimentological data of core GeoTü SL112 are stored in the Pangaea data base at the Alfred Wegener Institute at Bremerhaven, Germany (www.pangaea.de).

Modern clay mineral distribution

The compilation of published clay mineral data from the south-eastern Levantine Sea and adjacent areas provides a general picture of clay mineral supplies by dust-bearing winds, wadis and rivers (Figs. 1a, b, 2; Table 1). We distinguished two clay mineral assemblages for dust and four fluvial assemblages, which can be attributed to river and wadi systems draining the borderlands of the southeastern Levantine Sea. The assemblage of the SE Levantine Sea results from mixing of the other assemblages.

I. Northern Dust Assemblage

Aeolian dust samples collected in the vicinity of Cyprus during northerly to northwesterly winds have up to 54% illite, >20% smectite, >20% kaolinite and <10% chlorite (Figs. 1a, 2; Table 1). These sediments have potential sources in the northern Mediterranean hinterland, such as Turkey, Greece, and the Aegean islands (Chester et al., 1977). Illite and chlorite are mainly provided by weathering of metamorphic rocks, flysch, and molasse sediments of the Balkans (see compilation by Ehrmann et al., 2007a), and of metamorphic and sedimentary outcrops in Turkey, such as the Menderes Massif (Rimmelé et al., 2003). Smectite and kaolinite result from the weathering of Quaternary volcanic and sedimentary units (Gevrek and Kazanci, 2000; Karakas and Kadir, 2000; Innocenti et al., 2005).

II. Saharan Dust Assemblage

The samples of the Saharan Dust Assemblage collected over the Levantine Sea and the north African continent are characterized by variable dominance of kaolinite, illite and smectite (Figs. 1a, 2; Table 1). Some samples possess 10–15% palygorskite, which is commonly used as a tracer for aeolian dust derived from North Africa (Coudé-Gaussen and Blanc, 1985; Guerzoni et al., 1999; Foucault and Mélières, 2000; Goudie and Middleton, 2001). Kaolinite contributes with up to 50% to dust from the south and central Sahara (Chester et al., 1977; Foucault and Mélières, 2000; Goudie and Middleton, 2001). Kaolinite is an abundant clay mineral in the Cretaceous Nubian sandstone, in lateritic soils and, in particular, in deposits of the Fayoum depression south of Cairo (El-Sherbini and Issa, 1989; Stanley and Wingerath, 1996). Widespread outcrops of Paleocene and Eocene sediments in the northernmost part of Africa are additional sources (Bolle et al., 2000). North African illite occurrences are reported by Singer (1988) from desert loess deposits. Caquineau et al. (1998) point out that illite dominates the dust sources in the North and West Sahara, whereas kaolinite occurs mainly in the dust sources of the southern and central parts. Smectite is probably provided by weathering of Tertiary volcanic rocks, which crop out in east and central Africa.

III. Near East Assemblage

Suspended sediments transported by perennial and ephemeral rivers draining Gaza and Israel contain abundant amounts of smectite and kaolinite, which can reach concentrations of >70% and >30%, respectively. Illite occurs in variable amounts of around 10%, and contents of chlorite are lower (Figs. 1b, 2; Table 1).

Smectite may be derived from weathering of Miocene to recent volcanic rocks of the intraplate volcanic field Harrat Ash Shaam in Jordan and adjacent countries (Fig. 1a; Ibrahim et al., 2003; Shaw et al., 2003), tuff beds on Mt. Carmel near Haifa, and early Cretaceous volcanic rocks and shales in north Israel (Stanley et al., 1997; Sandler and Herut, 2000; Segev et al., 2005). Erosion of kaolinite-bearing soils and sediments, mainly of the Mesozoic Nubian sandstone formation (Stanley et al., 1997; Lado and Ben-Hur, 2004) may provide kaolinite. In particular, in the coastal-plain red soils the kaolinite concentrations may exceed those of smectite (Sandler and Herut, 2000). Small metamorphic areas in the central and southern part of Israel (Gur et al., 1995; Katz et al., 2004) may provide some illite and chlorite. Further potential illite and chlorite sources are Cretaceous (Stanley et al., 1997), Triassic (Heller-Kallai et al., 1973) and Palaeozoic sediments in the Negev (Heller-Kallai and Kalman, 1972; Stanley et al., 1997).

IV. Sinai Assemblage

Compared to the Near East Assemblage, kaolinite and illite are much more abundant in the Sinai Assemblage, with more than 40% and 20–30%, respectively. Smectite, in contrast, shows significantly lower concentrations of ca. 30%. Chlorite occurs in low amounts but was not quantified (Figs. 1b, 2; Table 1).

The assemblage is dominated by the sediment supply of Wadi El-Arish, which drains the Sinai and cuts mainly through Palaeozoic sediments. The kaolinite dominance is attributed to the erosion of Cambrian, Cretaceous, Tertiary and Quaternary sediments of the central part of the Sinai (Grindy and Tamish, 1985; Stanley et al., 1997; Wanas and Soliman, 2001). Smectite probably has its origin in small outcrops of basalts in the eastern part of the Sinai (Segev et al., 2005) and in weathered Cretaceous shales and marls (Stanley et al., 1997). Illite is derived from Cretaceous and Eocene shales, from the Syrian

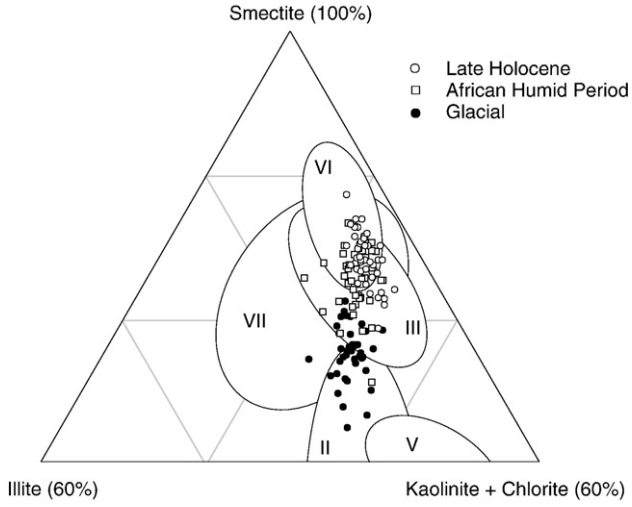

Figure 4. Ternary diagram showing the clay mineral composition of the late Quaternary sediments of core GeoTü SL112, subdivided into the glacial interval (41 samples), the African Humid Period (44 samples) and the late Holocene (48 samples). The clusters of the modern clay mineral assemblages in the southeastern Levantine Sea region are reproduced from Figure 2 for comparison. II Saharan Dust Assemblage, III Near East Assemblage, V Egyptian Wadi Assemblage, VI Nile Assemblage, VII SE Levantine Sea Assemblage. The fields of the Northern Dust Assemblage (I) and the Sinai Assemblage (IV) plot outside the chosen sector.

https://doi.org/10.1016/j.yqres.2009.01.001 Published online by Cambridge University Press

Arc in the northern and central part of the Sinai (Rosenthal et al., 1998; Cosca et al., 1999; Refaat and Imam, 1999; Kusky and El-Baz, 2000), and from Triassic sediments in southern Israel (Heller-Kallai et al., 1973). Minor occurrences of chlorite, as alteration product of andesites, are documented by El-Sayed (2006) in the northwest of the Sinai.

V. Egyptian Wadi Assemblage

The Egyptian Wadi Assemblage mirrors the sediment supply of wadis, which discharge into the Nile River. Similar to the Sinai Assemblage, kaolinite is most common with concentrations of 40–55%, followed by smectite with 35–45% and illite with 7–18%. Chlorite concentrations were not determined (Figs. 1b, 2; Table 1).

The wadis drain Eocene and Mesozoic sedimentary regions and the Red Sea Hills, which are dominated by Precambrian crystalline basement with volcanic rocks. Kaolinite is attributed to the erosion of Eocene and Mesozoic shales, marls and calcarenites, which contain up to 70% kaolinite (Bolle et al., 2000). The volcanic rocks of the Red Sea Hills are potential sources for smectite (Babiker and Gudmundsson, 2004). Possible sources for illite are Precambrian basement rocks of the Red Sea Hills and Eocene and Mesozoic sediments (Bolle et al., 2000; Babiker and Gudmundsson, 2004).

VI. Nile Assemblage

Smectite is the most dominant clay mineral of the Nile Assemblage, with values up to 85%. Kaolinite shows concentrations of about 20%. Illite contents are <10% and are therefore lower than in all other assemblages. Chlorite occurs in traces (Figs. 1b, 2; Table 1).

The Blue Nile and the Atbara River control the sediment load of the Nile River, whereas the White Nile is of secondary importance. The Blue Nile and the Atbara River cut through Cenozoic volcanic provinces of the Highland of Ethiopia (Ukstins et al., 2002), where smectite is provided in large quantities by chemical weathering (Venkatarathnam and Ryan, 1971; Maldonado and Stanley, 1981; Stanley and Wingerath, 1996; Foucault and Mélières, 2000). Kaolinite is mainly provided by Egyptian wadis, by the erosion of Eocene and Mesozoic sediments and lateritic soils, and by wind-borne supply (Venkatarathnam and Ryan, 1971; Stanley and Wingerath, 1996; Bolle et al., 2000). Illite and small amounts of chlorite come from nearby Cenozoic and Mesozoic sediments and possibly of Proterozoic rocks in the Red Sea Hills (Stanley and Wingerath, 1996; Bolle et al., 2000).

VII. SE Levantine Sea Assemblage

The sediment surface samples of the southeastern Levantine Sea show a relatively homogeneous clay mineral composition with a clear dominance of smectite, which can reach concentrations of >70%. The second-most important clay mineral is kaolinite with concentrations between ca. 10% and 30%, followed by illite with average values of 12%. Chlorite occurs in minor amounts of <10% (Figs. 1b, 2; Table 1).

The SE Levantine Sea Assemblage exhibits a mixed signal, influenced by the riverine influx from the North African continent and the Near East, and various sources of aeolian dust. The high concentrations of smectite document the dominant role of the sediment input by the Nile River (e.g., Venkatarathnam and Ryan, 1971; Maldonado and Stanley, 1981; Stanley and Wingerath, 1996; Stanley et al., 1997; Krom et al., 1999; Sandler and Herut, 2000). The smectite concentrations are highest along the flow path of the MSW. High concentrations of kaolinite and illite are found in the western part of the study area rather than in the eastern part. Saharan dust is a source delivering illite and kaolinite. However, the estimated modern aeolian dust rates are only of secondary importance compared with the sediment discharge by the Nile River (Ganor and Mamane, 1982; Goudie and Middleton, 2001). Isotopic geochemical and grain-size analyses of sediments in the region of site SL112 showed that >70% of the carbonate-free surface sediment is derived from the Nile River (Krom et al., 1999; Schilman et al., 2001; Hamann et al., 2008).

Clay mineral distribution during the late Quaternary

The late Quaternary sediments recovered with core GeoTü SL112 from the continental slope off Israel show distinct changes in the clay mineral composition through time (Figs. 3, 4). They obviously reflect changes in the source area, weathering and transport processes, which in turn were controlled by climate.

The glacial period

The glacial interval of core SL112 has the lowest sedimentation rates (ca. 14 cm/ka) of the core. The clay mineral composition distinctly differs from that of the Holocene sediments (Fig. 3). The glacial samples plot into the field of the modern SE Levantine Sea Assemblage and also overlap with the fields of the Saharan Dust Assemblage and the Near East Assemblage (Fig. 4).

The relatively high concentrations of kaolinite and illite indicate an intense influx of dust-bearing Saharan winds. Kaolinite theoretically also could originate from the Egyptian wadis. This, however, is not very likely because of the low activity of the wadis during the glacial period (Adamson et al., 1980). The high proportion of the mainly wind-transported clay minerals corresponds well with the dry and cool climate, as documented in East African lake and terrestrial climate records (e.g., Bonnefille and Charlié, 2000; Gasse, 2000; Gvirtzman and Wieder, 2001; Beuning et al., 2002). Although riverine sediment input was still significant, aeolian sediment components in the carbonate-free sediment fraction of SL112 compose 15–40% in the glacial interval, compared to only ca. 5% in the late Holocene (Hamann et al., 2008). Kohfeld and Harrison (2001) estimated that glacial dust accumulation in the Sahara/Sahel region was two to five times higher than in the late Holocene.

The low sedimentation rates and low smectite concentrations indicate a reduced influx of Nile suspension load. Some smectite was probably supplied from the Near East, especially during the LGM. Evidence for high moisture availability has been suggested by lake-level highstands of the Lake Lisan/Dead Sea system (Landmann et al., 2002).

Chlorite was found in the present discharge of the Nile River in only minor amounts, but was probably more important during the glacial due to an enhanced chlorite formation by physical weathering of metamorphosed Precambrian sequences (e.g., Beyth et al., 2003).

At the end of the glacial, an increase in the illite content to up to 18% is visible during the time of Heinrich Event 1 at ca. 16 cal ka BP (Fig. 3). Heinrich Events (e.g., Bond et al., 1993; Vidal et al., 1997) caused a strengthening of northwesterlies and increased northward Saharan dust transport into the Western Mediterranean Sea (e.g., Cacho et al., 2000; Moreno et al., 2002) and the Eastern Mediterranean Sea (Neev and Emery, 1995; Hamann et al., 2008). The observed change in the clay mineral assemblage implies particularly dry conditions in the source area and/or effective wind transport at the time of Heinrich Event 1. Additional evidence for Heinrich Event 1-related drought in the Eastern Mediterranean Sea comes from speleothem data, significant lake level drops of Lake Lisan/Dead Sea (Bar-Matthews et al., 1999; Bartov et al., 2003). Also, Lake Victoria and Lake Tana, which feed the White and Blue Nile, respectively, desiccated during this period (Talbot and Laerdal, 2000; Lamb et al., 2007). Therefore, one can assume a strongly reduced discharge of the Nile River.

The impact of Heinrich Event 2 at ca. 25 ka on the clay mineral record of SL112 is much less evident (Fig. 3). Heinrich Event 2 is also recorded by a modest coarsening of grain size (Hamann et al., 2008), which suggests a slight increase in aeolian activity. A lower amplitude

https://doi.org/10.1016/j.yqres.2009.01.001 Published online by Cambridge University Press

Heinrich Event 2 when compared to Heinrich Event 1 is consistent with differences in lake level lowering in the Lake Lisan/Dead Sea (Landmann et al., 2002).

The African Humid Period

After the glacial period, the climate of the North African continent ameliorated at about 15 cal ka BP to persistently humid conditions, the so-called African Humid Period, which lasted until ca. 5.5 cal ka BP (deMenocal et al., 2000a). The onset of the AHP was accompanied by a distinct change in the clay mineral composition near the base of the Bølling–Allerød (Fig. 3). Smectite concentrations increased, whereas illite, kaolinite and chlorite concentrations decreased. The samples of the AHP plot into the field of the modern SE Levantine Sea Assemblage and the Near East Assemblage. In contrast to the samples of the glacial period, they also overlap with the Nile Assemblage (Fig. 4). Thus, we attribute the change in clay mineralogy mainly to an enhanced influence of the Nile River and a concurrent decrease in Saharan dust.

Increased rainfall was the result of a strengthening of the African monsoon and a more northerly position of the ITCZ, which influenced wide areas across North Africa (e.g., deMenocal et al., 2000a; Renssen et al., 2006) and led to increased delivery of smectite. A Near East source may also have contributed to the smectite increase, because climatic ameliorations in this region also started at ca. 15 ka (Bar-Matthews et al., 1997; Landmann et al., 2002). However, this smectite source certainly was much less important than the Nile River. Aeolian sediment transport decreased by about 50%, due to an increased vegetation cover as documented in several records in North Africa (e.g., Adamson et al., 1980; Rossignol-Strick, 1999; deMenocal et al., 2000b; Renssen et al., 2006). The lower chlorite contents possibly indicate a change of the weathering regime to chemical rather than physical weathering caused by warmer and more humid conditions.

A short-term and minor decrease of smectite and kaolinite and an increase of illite concentrations centered at 12 cal ka BP may be related to a brief return to glacial-like conditions during the Younger Dryas which is characterized by enhanced aridity and increased dust flux rates, as also documented by several palynological, palaeosol, lake level, and grain-size analyses in the Mediterranean region (e.g., Bottema, 1995; Rossignol-Strick, 1995; Gasse, 2000; Gvirtzman and Wieder, 2001; Hamann et al., 2008). The dust influx, however, was characterized by low kaolinite contents and thus differs from that during the glacial and the late Holocene period, indicating a different source. Kaolinite occurs mainly in the central part of the Saharan desert, whereas illite dominates dust sources in its northern part (Caquineau et al., 1998; Goudie and Middleton, 2001).

Kaolinite abundance increased again to higher values throughout the early and mid-Holocene, but did not reach glacial concentrations. In contrast to the glacial period, when kaolinite entered the south-eastern Levantine Sea probably mainly by dust, wadis with kaolinite-enriched discharge were activated during the AHP by enhanced rainfall.

The smectite concentrations show no significant change during the time of sapropel S1 formation (9.6–6.5 cal ka BP), which is best explained by an overlap of the AHP signal with relatively constant and high outflow of suspended material by the Nile River.

The late Holocene

The abrupt end of the AHP and switch to arid conditions at 5.5 cal ka BP reported by various West African records (e.g., Claussen et al., 1999; deMenocal et al., 2000a; Kuhlmann et al., 2004) is not visible in SL112. In contrast, our data show a maximum Nile discharge at 4 cal ka BP with >70% smectite, the highest concentrations throughout the core. The late Holocene interval generally has a very similar clay mineral composition as the AHP interval, leading to a broad overlap between the two groups in the ternary diagram (Fig. 4). The linear sedimentation rate increased to maximum values in the range 32–36 cm/ka (Fig. 3). Starting at 4 cal ka BP smectite concentrations fell, reflecting a gradual reduction of smectite delivery by the Nile River to a minimum of 60% at 2 cal ka BP. A similar pattern in the smectite occurrence is documented in the southern Aegean Sea (Ehrmann et al., 2007b). Kaolinite shows an increase of concentrations from ca. 4 ka until ca. 1 ka to values of ca. 20%. This is attributed to a gradual aridification of the source area with enhanced aeolian transport of kaolinite-bearing dust rather than delivery of kaolinite by Egyptian wadis, given the limited activity of wadis during more arid conditions (Adamson et al., 1980; Stanley et al., 1997). Consequently, our data suggest a persistent maximum of Nile River discharge with humid conditions in East Africa until 4 cal ka BP. The climate transition from humid into arid conditions occurs gradually and more than 1000 yr after the end of AHP as documented in the West African climate records.

Our results are in line with results from Lake Yoa (northern Chad), which show a gradual termination of the AHP and a strong reduction of vegetation that allowed dust mobilization from ca. 4.3 cal ka BP (Kröpelin et al., 2008). The comparison of West African versus East African climate records reflects significant variations in their longitudinal and/or latitudinal patterns. This suggests a decoupling of the involved climate drivers. Simulations of the climatic evolution in Northern Africa during the Holocene clearly highlight regional differences in rainfall patterns and the related vegetation cover (Renssen et al., 2006). The West Sahara model defines distinct intervals of a green state (up to ca. 7.5 ka), a zone of instability (7.5 to 5.5 ka) and a desert state (5.5 ka to the present). It also reproduces the rapid climatic changes during onset and end of the AHP. In contrast, the impact of enhanced African monsoonal activity on the eastern Sahara is reflected by a more gradual response of the vegetation (Renssen et al., 2006; Kröpelin et al., 2008). These geographic differences may reflect the direct influence of oceanographic changes in the Indian Ocean on East Africa, as discussed below.

Mechanisms of fluctuations in the Nile River discharge

The comparison of the clay mineral record of this study with other palaeoclimatic data from the African continent and adjacent regions highlights the complexity of the regional climate evolution and history (e.g., reviews in Gasse, 2000; Mayewski et al., 2004; Robinson et al., 2006).

The fluctuating smectite concentrations reflect the general pattern of the Nile River discharge, which is to a large degree controlled by East African climate conditions. The comparison of the smectite concentrations of core SL112 with sea-surface temperatures (SST) in the Mozambique Channel (Fig. 3; Bard et al., 1997) shows remarkable similarities between both records. This relationship suggests a more-or-less direct link between fluctuations in the Blue Nile River discharge and sea-surface temperature evolution and climate oscillations in the tropical Indian Ocean, which is the key moisture source for the equatorial to northern East Africa (e.g., Giannini et al., 2005). Intervals of lower SSTs in the western part of the Indian Ocean, e.g., the glacial period, are probably associated with reduced rainfall and drought events of the Nile catchment area, a situation as seen during negative Indian Ocean Dipole events (IOD) (Saji and Yamagata, 2003). The IOD is tightly linked to the African/Asian monsoonal activity (e.g., Ashok et al., 2001; Ashok et al., 2004; Tierney et al., 2008), which is linked to the mean latitudinal position of the ITCZ (e.g., Haug et al., 2001; Fleitmann et al., 2003), and related to the evolution of ENSO patterns during past millennia (Ashok et al., 2004; Abram et al., 2007). An analogue scenario of a positive IOD-like event occurs during warmer SSTs in the western part of the Indian Ocean, for example during the early to mid-Holocene. Increased SSTs require increased convective activity with regard to an increase in rainfall in the adjacent African mainland, which affects the catchment areas of the

https://doi.org/10.1016/j.yqres.2009.01.001 Published online by Cambridge University Press

Nile tributaries (Abram et al., 2007). Modern studies of rainfall anomalies in central Africa show an increase in precipitation during positive IOD phases (Saji and Yamagata, 2003). Furthermore, our smectite record shows a remarkable correlation with the abundance of terrigenous matter in the western Arabian Sea, which consists largely of wind-derived dust from the Arabian Desert (Sirocko et al., 1996, Fig. 3). The similarities between the records underline the teleconnection between the monsoon system and the precipitation in East Africa.

In summary, our data suggest a tight coupling between Indian Ocean SST as the main moisture source for rainfall in east and northeast Africa (Fig. 3; Sirocko et al., 1996; Bard et al., 1997; Tierney et al., 2008). They provide additional support for a direct connection between the large-scale ocean atmosphere oscillatory modes IOD and ENSO and the mean annual position of the ITCZ with rainfall patterns in East Africa, which are ultimately responsible for the discharge of the Nile River.

Hence, the differences of West versus East African climate signals during the onset and end of the AHP may be related to different oceanographic scenarios in the Atlantic and Indian oceans. We suggest that the climate evolution in East Africa and the evolution of the Nile River discharge are mainly influenced by the Indian Ocean.

Conclusions

Our review of the modern clay mineral distribution around the southeastern Levantine Sea allows the identification of several source areas. Dust samples can be grouped into two assemblages. The Northern Dust Assemblage comprises aeolian sediments from the northeastern hinterland, with >40% illite, >20% smectite and >20% kaolinite. The Saharan Dust Assemblage shows a wide range of clay mineral compositions with up to 50% kaolinite and 15% palygorskite.

River and wadi sediments allow the discrimination of four fluvial assemblages. The Near East Assemblage consists of >40% smectite and mean kaolinite concentrations of 30%. The Sinai Assemblage is dominated by some 50% kaolinite, <30% smectite and <30% illite. The Egyptian Wadi Assemblage has similar kaolinite contents but higher smectite concentrations of ca. 40%. The Nile Assemblage is characterized by a distinct smectite dominance of 65%–85%.

The marine SE Levantine Sea clay mineral assemblage reveals a mixture of the other assemblages, with a dominance of smectite (40–75%) over illite (5–25%) and kaolinite (10–30%).

Changes in the late Quaternary clay mineral distribution in the southeastern Levantine Sea were caused by changes in the source areas, weathering processes and transport regimes as a consequence of changing climatic conditions. The sedimentation pattern of the glacial period was mainly controlled by the general cold and dry climate with enhanced aeolian transport of Saharan dust and reduced fluviatile discharge, as indicated by high kaolinite and illite but low smectite concentrations. Heinrich-equivalent signals are reflected in higher illite concentrations at ca. 16 ka and 25 ka, which point to an increased wind intensity. Heinrich Event 2 is much less pronounced than Heinrich Event 1.

The high smectite concentrations during the AHP suggest an increased discharge of the Nile River due to humid conditions. In contrast to West African records, a more gradual onset of the AHP is documented in the southeastern Levantine Sea. Also the end of the AHP is transitional and occurs at about 4 cal ka BP. Hence, this climate transition postdates the abrupt climate shift of West Africa by more than 1000 yr. The general trend to modern arid conditions with broad desert zones in Africa, reduced fluvial activity and high aeolian fluxes is indicated by a decline of smectite concentrations, which suggests slightly decreasing Nile River discharge rates during the past 4 ka.

The longer-term trend of the smectite concentration in core SL112 shows a relationship with the Indian Ocean sea-surface temperatures record derived from the Mozambique Channel and a monsoon record from the western Arabian Sea, and suggests a direct forcing of the hydrological balance of the Nile River due to oceanographic changes in the Indian Ocean.

Acknowledgments

Sediment core GeoTü SL112 was collected during R/V *Meteor* cruise M51/3 in 2001. We thank the captain, the crew and the chief scientist C. Hemleben (Tübingen) for recovering and providing the core for this study. Furthermore we thank S. Dorn and Y. Milker (Leipzig) for their assistance in the laboratories, and P.M. Grootes (Kiel) for age determinations. We acknowledge the constructive criticism by B. Dieckmann, an anonymous reviewer and the editors, which helped improve the manuscript. This project was financially supported by the German Research Council (DFG).

References

Abram, N.J., Gagan, M.K., Liu, Z., Hantoro, W.S., McCulloch, M.T., Suwargadi, B.W., 2007. Seasonal characteristics of the Indian Ocean Dipole during the Holocene epoch. Nature 445, 299–302.

Adamson, D.A., Gasse, F., Street, F.A., Williams, M.A.J., 1980. Late Quaternary history of the Nile. Nature 288, 50–55.

Aksu, A., Yasar, D., Mudie, P.J., 1995. Paleoclimatic and paleoceanographic conditions leading to development of Sapropel layer S1 in the Aegean Sea. Palaeogeography Palaeoclimatology Palaeoecology 116, 71–101.

Ashok, K., Guan, Z., Yamagata, T., 2001. Impact of the Indian Ocean Dipole on the relationship between the Indian monsoon rainfall and ENSO. Geophysical Research Letters 28, 4499–4502.

Ashok, K., Guan, Z., Saji, N.H., Yamagata, T., 2004. Individual and combined influences of ENSO and the Indian Ocean Dipole on the Indian Summer Monsoon. Journal of Climate 17, 3141–3155.

Babiker, M., Gudmundsson, A., 2004. The effects of dykes and faults on groundwater flow in an arid land: the Red Sea Hills, Sudan. Journal of Hydrology 297, 256–273.

Bard, E., Rostek, F., Sonzogni, C., 1997. Interhemispheric synchrony of the last deglaciation inferred from alkenone palaeothermometry. Nature 385, 707–710.

Bar-Matthews, M., Ayalon, A., Kaufman, A., 1997. Late Quaternary paleoclimate in the Eastern Mediterranean Region from Stable Isotope Analysis of Speleothems at Soreq Cave, Israel. Quaternary Research 47, 155–168.

Bar-Matthews, M., Ayalon, A., Kaufman, A., Wasserburg, G.J., 1999. The Eastern Mediterranean paleoclimate as a reflection of regional events: Soreq cave, Israel. Earth and Planetary Science Letters 166, 85–95.

Bartov, Y., Goldstein, S.L., Stein, M., Enzel, Y., 2003. Catastrophic arid episodes in the Eastern Mediterranean linked with the North Atlantic Heinrich events. Geology 31, 439–442.

Beuning, K.R.M., Kelts, K., Russell, J., Wolfe, B.B., 2002. Reassessment of Lake Victoria-Upper Nile River paleohydrology from oxygen isotope records of lake-sediment cellulose. Geology 30, 559–562.

Beyth, M., Avigad, D., Wetzel, H.-U., Matthews, A., Berhe, S.M., 2003. Crustal exhumation and indications for Snowball Earth in the East African Orogen: north Ethiopia and east Eritrea. Precambrian Research 123, 187–201.

Biscaye, P.E., 1965. Mineralogy and sedimentation of recent deep sea clay in the Atlantic Ocean and adjacent seas and oceans. Geological Society of America Bulletin 76, 803–832.

Bolle, M.-P., Tantawy, A.A., Pardo, A., Adatte, T., Burns, S., Kassab, A., 2000. Climatic and environmental changes documented in the upper Paleocene to lower Eocene of Egypt. Ecologae Geologicae Helvetiae. 93, 33–51.

Bond, G., Broecker, W.S., Johnsen, S.J., McManus, J.F., Labeyrie, L., Jouzel, J., Bonani, G., 1993. Correlation between climate records from North Atlantic sediments and Greenland ice. Nature 365, 143–147.

Bonnefille, R., Chalie, F., 2000. Pollen-inferred precipitation time-series from equatorial mountains, Africa, the last 40 kyr BP. Global and Planetary Change 26, 25–50.

Bottema, S., 1995. The Younger Dryas in the Eastern Mediterranean. Quaternary Science Reviews 14, 883–891.

Cacho, I., Grimalt, J.O., Sierro, F.J., Shackleton, N., Canals, M., 2000. Evidence for enhanced Mediterranean thermohaline circulation during rapid climatic coolings. Earth and Planetary Science Letters 183, 417–429.

Camuffo, D., 1993. Controlling the aeolian erosion of the Great Sphinx. Studies in Conservation 38, 198–205.

Caquineau, S., Gaudichet, A., Gomes, L., Magonthier, M.-C., Chatenet, B., 1998. Saharan dust: clay ratio as a relevant tracer to assess the origin of soil-derived aerosols. Geophysical Research Letters 25, 983–986.

Chester, R., Baxter, G.G., Behairy, A.K.A., Connor, K., Cross, D., Elderfield, H., Padgham, R.C., 1977. Soil-sized eolian dust from the lower troposphere of the Eastern Mediterranean Sea. Marine Geology 24, 201–217.

Claussen, M., Kubatzki, C., Brovkin, V., Ganopolski, A., Hoelzmann, P., Pachur, H.-J., 1999. Simulation of an abrupt change in Saharan vegetation in the mid-Holocene. Geophysical Research Letters 26, 2037–2040.

Cosca, M.A., Shimron, A., Caby, R., 1999. Late Precambrian metamorphism and cooling in the Arabian-Nubian Shield: petrology and $^{40}Ar/^{39}Ar$ geochronology of metamorphic rocks of the Elat area (southern Israel). Precambrian Research 98, 107–127.

https://doi.org/10.1016/j.yqres.2009.01.001 Published online by Cambridge University Press

Coudé-Gaussen, G., 1981. Etude détaillée d'un échantillon de poussières éolinnes prélevé au Tanezrouft, le 10 décembre 1980. Recherches Géographiques à Strasbourg 16/17, 121–130.
Coudé-Gaussen, G., Blanc, P., 1985. Présence de grains éolisés de palygorskite dans les poussières actuelles et les sédiments rècents d'origine désertique. Bulletin de la Société Géologique de France 8, 283–292.
deMenocal, P., Ortiz, J., Guilderson, T., Adkins, J., Sarnthein, M., Baker, L., Yarusinsky, M., 2000a. Abrupt onset and termination of the African Humid Period: rapid climate responses to gradual insolation forcing. Quaternary Science Reviews 19, 347–361.
deMenocal, P., Ortiz, J., Guilderson, T., Sarnthein, M., 2000b. Coherent high- and low-latitude climate variability during the Holocene warm period. Science 288, 2198–2202.
Ehrmann, W., Schmiedl, G., Hamann, Y., Kuhnt, T., 2007a. Distribution of clay minerals in surface sediments of the Aegean Sea: a compilation. International Journal of Earth Sciences 96, 769–780.
Ehrmann, W., Schmiedl, G., Hamann, Y., Kuhnt, T., Hemleben, C., Siebel, W., 2007b. Clay minerals in late glacial and Holocene sediments of the northern and southern Aegean Sea. Palaeogeography Palaeoclimatology Palaeoecology. 249, 36–57.
El-Sayed, M.M., 2006. Geochemistry and petrogenesis of the post-orogenic bimodal dyke swarms in NW Sinai, Egypt: constraints on the magmatic-tectonic processes during the late Precambrian. Chemie der Erde 66, 129–141.
El-Sherbini, M.I., Issa, G.I., 1989. Composition and origin of some calcrete deposits in south Western Desert of Egypt. Journal of African Earth Sciences 9, 461–466.
Fairbanks, R.G., Mortlock, R.A., Chiu, T.-C., Cao, L., Kaplan, A., Guilderson, T.P., Fairbanks, T.W., Bloom, A.L., Grootes, P.M., Nadeau, M.-J., 2005. Radiocarbon calibration curve spanning 0 to 50,000 years BP based on paired $^{230}Th/^{234}U/^{238}U$ and ^{14}C dates on pristin corals. Quaternary Science Reviews 24, 1781–1796.
Fleitmann, D., Burns, S.J., Mudelsee, M., Neff, U., Kramers, J., Mangini, A., Matter, A., 2003. Holocene forcing of the Indian monsoon recorded in a stalagmite from Southern Oman. Science 300, 1737–1739.
Foucault, A., Mélières, F., 2000. Palaeoclimatic cyclicity in central Mediterranean Pliocene sediments: the mineralogical signal. Palaeogeography Palaeoclimatology Palaeoecology 158, 311–323.
Giannini, A., Saravanan, R., Chang, P., 2005. Dynamics of the boreal summer African monsoon in the NSIPP1 atmospheric model. Climate Dynamics 25, 517–535.
Ganor, E., Mamane, Y., 1982. Transport of Saharan dust across the Eastern Mediterranean. Atmospheric Environment 16, 581–587.
Garzanti, E., Ando, S., Vezzoli, G., Abdel Megid, A.A., El Kammar, A., 2006. Petrology of Nile River sands (Ethiopia and Sudan): sediment budgets and erosion patterns. Earth and Planetary Science Letters 252, 327–341.
Gasse, F., 2000. Hydrological changes in the African tropics since the Last Glacial Maximum. Quaternary Science Reviews 19, 189–211.
Gevrek, A.I., Kazanci, N., 2000. A Pleistocene, pyroclastic-poor maar from central Anatolia, Turkey: influence of a local fault on a phreatomagmatic eruption. Journal of Volcanology and Geothermal Research 95, 309–317.
Goudie, A.S., Middleton, N.J., 2001. Saharan dust storms: nature and consequences. Earth-Science Reviews 56, 179–204.
Grindy, A.R., Tamish, M.M.O., 1985. Some major and trace constituents of Phanerozoic Egyptian mudrocks and marls. Journal of African Earth Sciences 3, 303–320.
Guerzoni, S., Chester, R., Dulac, F., Herut, B., Loye-Pilot, M.-D., Measures, C., Migon, C., Molinaroli, E., Moulin, C., Rossini, P., Saydam, C., Soudine, A., Ziveri, P., 1999. The role of atmospheric deposition in the biochemistry of the Mediterranean Sea. Progress in Oceanography 44, 147–190.
Gur, D., Steinitz, G., Kolodny, Y., Starinsky, A., McWilliams, M., 1995. $^{40}Ar/^{39}Ar$ dating of combustion metamorphism ("Mottled Zone", Israel). Chemical Geology 122, 171–184.
Gvirtzman, G., Wieder, M., 2001. Climate of the last 53,000 years in the eastern Mediterranean, based on soil-sequence stratigraphy in the coastal plain of Israel. Quaternary Science Reviews 20, 1827–1849.
Hamann, Y., Ehrmann, W., Schmiedl, G., Krüger, S., Stuut, J.-B.W., Kuhnt, T., 2008. Sedimentation processes in the Eastern Mediterranean Sea during the Late Glacial and Holocene revealed by end-member modelling of the terrigenous fraction in marine sediments. Marine Geology 248, 97–114.
Haug, G.H., Hughen, K.A., Sigman, D.M., Peterson, L.C., Röhl, U., 2001. Southward migration of the Intertropical Convergence Zone through the Holocene. Science 293, 1304–1308.
Heller-Kallai, L., Kalman, Z.H., 1972. Some naturally occurring illite-smectite interstratifications. Clay Clay Minerals 20, 165–168.
Heller-Kallai, L., Nathan, Y., Zak, I., 1973. Clay mineralogy of Triassic sediments in southern Israel and Sinai. Sedimentology 20, 513–521.
Hemleben, C., 2002. Short Cruise Report, R.V. Meteor Cruise 51, Leg 3 Valletta-Malta to Istanbul-Turkey 14.11.-10.12.2001.
Holeman, J.N., 1968. The sediment yield of major rivers of the world. Water Resources Research 4, 737–747.
Hurrell, J.W., Kushnir, Y., Ottersen, G., Visbeck, M., 2003. An overview of the North Atlantic Oscillation. Geophysical Monograph 134, 1–35.
Ibrahim, K.M., Tarawneh, K., Rabba, I., 2003. Phases of activity and geochemistry of basaltic dike systems in northeast Jordan parallel to the Red Sea. Journal of Asian Earth Sciences 21, 467–472.
Innocenti, F., Agostini, S., Di Vincenzo, G., Doglioni, C., Manetti, P., Savascin, M.Y., Tonarini, S., 2005. Neogene and Quaternary volcanism in Western Anatolia: magma sources and geodynamic evolution. Marine Geology 221, 397–421.
Janicot, S., Harzallah, A., Fontaine, B., Moron, V., 1997. West African monsoon dynamics and eastern equatorial Atlantic and Pacific SST Anomalies (1970–88). Journal of Climate 11, 1874–1882.
Joseph, J.H., Manes, A., Ashbel, D., 1973. Desert aerosols transported by Khamsinic depressions and their climatic effects. Journal of Applied Meterology 12, 792–797.
Karakas, Z., Kadir, S., 2000. Devitrification of volcanic glasses in Konya volcanic unit, Turkey. Turkish Journal of Earth Sciences 9, 39–46.
Katz, O., Beyth, M., Miller, N., Stern, R., Avigad, D., Basu, A., Anbar, A., 2004. A Late Neoproterozoic (~630 Ma) high-magnesium andesite suite from southern Israel: implications for the consolidation of Gondwanaland. Earth and Planetary Science Letters 218, 475–490.
Klein, B., Roether, W., Manca, B.B., Bregant, D., Beitzel, V., Kovacevic, V., Luchetta, A., 1999. The large deep water transient in the Eastern Mediterranean. Deep-Sea Research I 46, 371–414.
Kohfeld, K.E., Harrison, S.P., 2001. DIRTMAP: the geological record of dust. Earth-Science Reviews 54, 81–114.
Krom, M.D., Cliff, R.A., Eijsink, L.M., Herut, B., Chester, R., 1999. The characterisation of Saharan dusts and Nile particulate matter in surface sediments from the Levantine basin using Sr isotopes. Marine Geology 155, 319–330.
Kröpelin, S., Verschuren, D., Lezine, A.M., Eggermont, H., Cocquyt, C., Francus, P., Cazet, J.P., Fagot, M., Rumes, B., Russell, J.M., Darius, F., Conley, D.J., Schuster, M., von Suchodoletz, H., Engstrom, D.R., 2008. Climate-driven ecosystem succession in the Sahara: the past 6000 years. Science 320, 765–768.
Kuhlmann, H., Meggers, H., Freudenthal, T., Wefer, G., 2004. The transition of the monsoonal and N Atlantic climate system off NW Africa during the Holocene. Geophysical Research Letters 31, 1–4.
Kuhnt, T., Schmiedl, G., Ehrmann, W., Hamann, Y., Anderson, A., 2008. Stable isotopic composition of Holocene benthic foraminifers from the Eastern Mediterranean Sea: past changes in productivity and deep water oxygenation. Palaeogeography Palaeoclimatology Palaeoecology 268, 106–115.
Kusky, T., El-Baz, F., 2000. Neotectonics and fluvial geomorphology of the northern Sinai Peninsula. Journal of African Earth Sciences 31, 213–235.
Lado, M., Ben-Hur, M., 2004. Soil mineralogy effects on seal formation, runoff and soil loss. Applied Clay Science 248, 209–224.
Lamb, H.F., Bates, C.R., Coombes, P.V., Marshall, M.H., Umer, M., Davies, S.J., Dejen, E., 2007. Late Pleistocene desiccation of Lake Tana, source of the Blue Nile. Quaternary Science Reviews 26, 287–299.
Landmann, G., Abu Qudaira, G.H., Shawabkeh, K., Wrede, V., Kempe, S., 2002. Geochemistry of the Lisan and Damya Formation in Jordan, and implications for palaeoclimate. Quaternary International 89, 45–57.
Malanotte-Rizzoli, P., Hecht, A., 1988. Large-scale properties of the Eastern Mediterranean: a review. Oceanologica Acta 11, 323–335.
Maldonado, A., Stanley, D.J., 1981. Clay mineral distribution patterns as influenced by depositional processes in the Southeastern Levantine Sea. Sedimentology 28, 21–32.
Mayewski, P.A., Rohling, E.J., Stager, J.C., Karlén, W., Maasch, K.A., Meeker, L.D., Meyerson, E.A., Gasse, F., van Kreveld, S., Holmgren, K., Lee-Thorp, J., Rosqvist, G., Rack, F., Staubwasser, M., Schneider, R.R., Steig, E.J., 2004. Holocene climate variability. Quaternary Research 62, 243–255.
Milliman, J.D., Syvitski, J.P.M., 1992. Geomorphic/tectonic control of sediment discharge to the ocean: the importance of small mountainous rivers. Journal of Geology 100, 525–544.
Moreno, A., Cacho, I., Canals, M., Prins, M.A., Sanchez-Goni, M.-F., Grimalt, J.O., Weltje, G.J., 2002. Saharan dust transport and high-latitude glacial climatic variability: the Alboran Sea record. Quaternary Research 58, 318–328.
Neev, D., Emery, K.O., 1995. The Destruction of Sodom, Gomorrah, and Jericho: Geological, Climatological, and Archaeological Background. Oxford University Press, New York. 175 pp.
Paquet, H., Coude-Gaussen, G., Rognon, P., 1984. Etude mineralogique de poussieres le long d'un itineraire entre 19° et 35° de latitude nord. Revue de Geologie Dynamique et de Geographie Physique 25, 257–265.
Pickard, G.L., Emery, W.J., 1982. Descriptive Physical Oceanography — An Introduction. Pergamon Press, San Diego. 249 pp.
Pinardi, N., Masetti, E., 2000. Variability of the large scale general circulation of the Mediterranean Sea from observations and modelling: a review. Palaeogeography Palaeoclimatology Palaeoecology 158, 153–174.
Pye, K., 1992. Aeolian dust transport and deposition over Crete and adjacent parts of the Mediterranean Sea. Earth Surface Processes and Landforms 17, 271–288.
Refaat, A.A., Imam, M.M., 1999. The Tayiba Red Beds: transitional marine-continental deposits in the precursor Suez Rift, Sinai, Egypt. Journal of African Earth Sciences 28, 487–506.
Renssen, H., Brovkin, V., Fichefet, T., Goosse, H., 2006. Simulation of the Holocene climate evolution in Northern Africa: the termination of the African Humid Period. Quaternary International 150, 95–102.
Rimmelé, G., Oberhänsli, R., Goffé, B., Jolivet, L., Candan, O., Cetinkaplan, M., 2003. First evidence of high-pressure metamorphism in the "Cover Series" of the southern Menderes Massif. Tectonic and metamorphic implications for the evolution of SW Turkey. Lithos 71, 19–46.
Robinson, S.A., Black, S., Sellwood, B.W., Valdes, P.J., 2006. A review of palaeoclimates and palaeoenvironments in the Levant and Eastern Mediterranean from 25,000 to 5000 years BP: setting the environmental background for the evolution of human civilisation. Quaternary Science Reviews 25, 1517–1541.
Rosenthal, E., Jones, B.F., Weinberger, G., 1998. The chemical evolution of Kurnub Group paleowater in the Sinai-Negev province—a mass balance approach. Applied Geochemistry 13, 553–569.
Rossignol-Strick, M., 1995. Sea–land correlation of pollen records in the Eastern Mediterranean for the glacial–interglacial transition: biostratigraphy versus radiometric time-scale. Quaternary Science Reviews 14, 893–915.
Rossignol-Strick, M., 1999. The Holocene climatic optimum and pollen records of sapropel 1 in the eastern Mediterranean, 9000–6000 BP. Quaternary Science Reviews 18, 515–530.

Rossignol-Strick, M., Nesteroff, W., Olive, P., Vergnaud-Grazzini, C., 1982. After the deluge: Mediterranean stagnation and sapropel formation. Nature 295, 105–110.
Saaroni, H., Ziv, B., Bitan, A., Alpert, P., 1998. Easterly wind storms over Israel. Theoretical and Applied Climatology 59, 61–77.
Saji, N.H., Yamagata, T., 2003. Indian ocean dipole mode events and African rainfall variability. CLIVAR Exchanges 27, 1–4.
Saji, N.H., Goswami, B.N., Vinayachandran, P.N., Yamagata, T., 1999. A dipole mode in the tropical Indian Ocean. Nature 401, 360–363.
Sandler, A., Herut, B., 2000. Composition of clays along the continental shelf off Israel: contribution of the Nile versus local sources. Marine Geology 167, 339–354.
Schilman, B., Almogi-Labin, A., Bar-Matthews, M., Labeyrie, L., Paterne, M., Luz, B., 2001. Long- and short-term carbon fluctuations in the Eastern Mediterranean during the late Holocene. Geology 29, 1099–1102.
Schott, F.A., McCreary Jr., J.P., 2001. The monsoon circulation of the Indian Ocean. Progress in Oceanography 51, 1–123.
Segev, A., Weissbrod, T., Lang, B., 2005. $^{40}Ar/^{39}Ar$ dating of the Aptian-Albian igneous rocks in Makhtesh Ramon (Negev, Israel) and its stratigraphic implications. Cretaceous Research 26, 633–656.
Shaw, J.E., Baker, J.A., Menzies, M.A., Thirlwall, M.F., Ibrahim, K.M., 2003. Petrogenesis of the largest intraplate volcanic field on the Arabian Plate (Jordan): a mixed lithosphere–asthenosphere source activated by lithospheric extension. Journal of Petrology 44, 1657–1679.
Siani, G., Paterne, M., Michel, E., Sulpizio, R., Sbrana, A., Arnold, M., Haddad, G., 2001. Mediterranean Sea surface radiocarbon reservoir age changes since the last glacial maximum. Science 294, 1917–1920.
Singer, A., 1988. Illite in aridic soils, desert dusts and desert loess. Sedimentary Geology 59, 251–259.
Sirocko, F., Garbe-Schönberg, D., McIntyre, A., Molfino, B., 1996. Teleconnections between the subtropical monsoons and high-latitude climates during the last deglaciation. Science 272, 526–529.
Stanley, D.J., Galili, E., 1996. Sediment dispersal along northern Israel coast during the early Holocene: geological and archaeological evidence. Marine Geology 130, 11–17.
Stanley, D.J., Wingerath, J.G., 1996. Clay mineral distributions to interpret Nile cell provenance and dispersal: I. Lower River Nile to delta sector. Journal of Coastal Research 12, 911–929.
Stanley, D.J., Mart, Y., Nir, Y., 1997. Clay mineral distributions to interpret Nile cell provenance and dispersal: II. Coastal plain from Nile delta to Northern Israel. Journal of Coastal Research 13, 506–533.
Stuut, J.-B.W., Lamy, F., 2004. Climate variability at the southern boundaries of the Namib (southwestern Africa) and Atacama (northern Chile) coastal deserts during the last 120,000 yr. Quaternary Research 62, 301–309.
Talbot, M.R., Laerdal, T., 2000. The Late Pleistocene–Holocene palaeolimnology of Lake Victoria, East Africa, based upon elemental and isotopic analyses of sedimentary organic matter. Journal of Paleolimnology 23, 141–164.
Tierney, J.E., Russell, J., Huang, Y., Sinninghe Damste, J.S., Hopmans, E.C., Cohan, A.S., 2008. Northern Hemisphere controls on tropical southeast African climate during the past 60,000 years. Science 322, 252–255.
Tütken, T., Eisenhauer, A., Wiegand, B., Hansen, B.T., 2002. Glacial–interglacial cycles in Sr and Nd isotopic composition of Arctic marine sediments triggered by the Svalbard/Barents Sea ice sheet. Marine Geology 182, 351–372.
Ukstins, I.A., Renne, P.R., Wolfenden, E., Baker, J.A., Ayalew, D., Menzeis, M., 2002. Matching conjugate volcanic rifted margins: $^{40}Ar/^{39}Ar$ chrono-stratigraphy of pre- and syn-rift bimodal flood volcanism in Ethiopia and Yemen. Earth and Planetary Science Letters 198, 289–306.
Venkatarathnam, K., Ryan, W.B.F., 1971. Dispersal patterns of clay minerals in the sediments of the eastern Mediterranean Sea. Marine Geology 11, 261–282.
Vidal, L., Labeyrie, L., Cortijo, E., Arnold, M., Duplessy, J.C., Michel, E., Becqué, S., van Weering, T.C.E., 1997. Evidence for changes in the North Atlantic Deep Water linked to meltwater surges during the Heinrich events. Earth and Planetary Science Letters 146, 13–27.
Wanas, H.A., Soliman, H.E., 2001. Allogenic and authigenic clays of the Lower Palaeozoic sandstones of the Naqus Formation at Gebel Gunna, central Sinai, Egypt: their recognition and geological significance. Journal of African Earth Sciences 32, 47–60.
Webster, P.J., Moore, A.M., Loschnigg, J.P., Leben, R.R., 1999. Coupled ocean–atmosphere dynamics in the Indian Ocean during 1997–98. Nature 401, 356–360.
Weldeab, S., Emeis, K.-C., Hemleben, C., Siebel, W., 2002a. Provenance of lithogenic surface sediments and pathways of riverine suspended matter in the Eastern Mediterranean Sea: evidence from $^{143}Nd/^{144}Nd$ and $^{87}Sr/^{96}Sr$ ratios. Chemical Geology 186, 139–149.
Weldeab, S., Emeis, K.-C., Hemleben, C., Vennemann, T.W., Schulz, H., 2002b. Sr and Nd isotope composition of Late Pleistocene sapropels and nonsapropelic sediments from the Eastern Mediterranean Sea: implications for detrital influx and climatic conditions in the source areas. Geochimica et Cosmochimica Acta 66, 3585–3598.
Williams, M., Talbot, M.R., Aharon, P., Salaam, Y.A., Williams, F., Brendeland, N.I., 2006. Abrupt return of the summer monsoon 15,000 years ago: new supporting evidence from the lower White Nile valley and Lake Albert. Quaternary Science Reviews 25, 2651–2665.
Wüst, G., 1960. Die Tiefenzirkulation des Mittelländischen Meeres in den Kernschichten des Zwischen- und des Tiefenwassers. Deutsche Hydrographische Zeitschrift 13, 105–131.
Wüst, G., 1961. On the vertical circulation of the Mediterranean Sea. Journal of Geophysical Research 66, 3261–3271.